Ultimate Signal-to-Noise-Ratio of Surface and Body Antennas for Magnetic Resonance Imaging

Wilfried Schnell, Wolfgang Renz, Markus Vester, and Helmut Ermert, *Senior Member, IEEE*

***Abstract*—Approximating the human body by a homogeneous half-space or cylinder the electromagnetic fields of surface antennas or wholebody antennas for magnetic resonance imaging (MRI) can analytically be calculated. Using these expressions the signal-to-noise ratio (SNR) of a general magnetic resonance detecting antenna can be predicted. We show how the optimum magnetic resonance antenna must look like to achieve the maximum SNR, which will also be presented. Finally, we apply the derived formulas to special antenna geometries like the single- and the double-loop coil, the magnetic dipole, and the "birdcage" resonator.**

***Index Terms*—Magnetic resonance, signal-to-noise ratio.**

I. Introduction

A. Brief History

ODAY, magnetic resonance imaging (MRI) is a common method for getting insights into the human body. The phenomenom of nuclear magnetic resonance (MR) was found by Bloch [1] and Purcell [2] in 1946; after stimulation, certain kinds of nuclei emit electromagnetic waves that can be detected by a radio frequency antenna (commonly named as an RF coil). The frequency f of the received RF signal depends on the kind of nucleus (with a certain gyromagnetic constant γ) and the strength of the static magnetic field $\boldsymbol{B}_0$, which is applied during the experiment: $2\pi f = \omega = |\gamma| B_0$. Thirty years later, a method was suggested to reconstruct tomographic images from MR signals recorded in presence of a magnetic field gradient [3], [4]. The quality of the reconstructed images depends strongly on the signal-to-noise-ratio (SNR) of the acquired MR signals. Thus, there is a substantial interest to design antennas providing the best possible SNR.

B. Calculation of the SNR

Basic research on the SNR of MR signals was conducted by Hoult together with Richards [5] and with Lauterbur [6]. In the first article, the noise was assumed to be solely produced by the antenna itself; in the second one, the sample was also considered as a noise source (with $k =$ Boltzmann's constant and $\Delta f =$ receiver bandwidth)

$$u_{N,\,\mathrm{eff}} = \sqrt{4kT\Delta f(R_A + R_L)}. \tag{1}$$

Manuscript received January 5, 1999; revised October 11, 1999.

W. Schnell is with the Marketing Technology Modules Department, Siemens Information and Communication Networks Group, Munich D-81359 Germany.

W. Renz and M. Vester are with the Magnetic Resonance Department, Siemens Medical Systems Group, Erlangen D-91052 Germany.

H. Ermert is with the Department of Electrical Engineering, Ruhr-University Bochum, Bochum D-44780 Germany.

Publisher Item Identifier S 0018-926X(00)02461-3.

It is assumed that the sample and the antenna are nearly at the same absolute temperature T. The real part of the input impedance of the antenna consists of R_L and R_A, which are related to the load (sample) and to the antenna itself, respectively. The calculation of the signal voltage U_S induced by a nuclear magnetization $\boldsymbol{M}$ (over a small volume V) was based on a specialization of the Lorentz reciprocity theorem (cf. [7] for details), which can be stated as follows:

$$U_S(\boldsymbol{r}) = -j\omega V \boldsymbol{M}\,\frac{\boldsymbol{B}(\boldsymbol{r})}{I}. \tag{2}$$

$\boldsymbol{B}(\boldsymbol{r})$ is the magnetic field which a coil with current I will produce at the point of interest $\boldsymbol{r}$ within the sample. Note that we use peak vectors for all time dependent values V in our calculations

$$\boldsymbol{V}(\boldsymbol{r}, t) = \mathrm{Re}\{\boldsymbol{V}(\boldsymbol{r}) e^{j\omega t}\}. \tag{3}$$

Combining (2) with (1) will yield an expression for the SNR of the measured signal generated by the nuclear magnetization $\boldsymbol{M}$ rotating perpendicularly to the static magnetic field $\boldsymbol{B}_0$ with the angular frequency $\omega = |\gamma| B_0$ ($\boldsymbol{M}$ is assumed to be homogeneous over the finite volume V located at the point of interest $\boldsymbol{r}$)

$$\begin{aligned}\left(\frac{S}{N}\right)(\boldsymbol{r}) &= \frac{|U_S(\boldsymbol{r})|}{\sqrt{2}u_{N,\,\mathrm{eff}}} \\ &= \frac{|\omega V \boldsymbol{M}\cdot\boldsymbol{B}(\boldsymbol{r})/I|}{\sqrt{8kT\Delta f(R_A + R_L)}} \\ &= \frac{\omega V|\boldsymbol{M}\cdot\boldsymbol{B}(\boldsymbol{r})|}{\sqrt{8kT\Delta f(R_A|I|^2 + R_L|I|^2)}} \\ &= \frac{\omega V|\boldsymbol{M}\cdot\boldsymbol{B}(\boldsymbol{r})|}{\sqrt{16kT\Delta f(P_A + P_L)}}.\end{aligned} \tag{4}$$

P_A and P_L are equal to the power loss within the antenna and the load, respectively, when the antenna carries a given current I or, more general, a given current distribution $\boldsymbol{K}$. The losses can be calculated by integration of the antenna current distribution $\boldsymbol{K}$ and of the resulting electric field $\boldsymbol{E}$ over the area of the antenna and over the volume of the load, respectively

$$P_A = \frac{1}{2\kappa_A d}\iint_{A'} \boldsymbol{K}\cdot\boldsymbol{K}^*\,dA' \tag{5}$$

$$P_L = \frac{\kappa_L}{2}\iiint_{V_L} \boldsymbol{E}\cdot\boldsymbol{E}^*\,dV. \tag{6}$$

d means the thickness of the antenna material and κ_A, κ_L are the conductivities of the antenna and the tissue, respectively.

Once $\boldsymbol{B}(\boldsymbol{r})$, P_L, and P_A are calculated, the SNR can be predicted. The calculation of these variables can be done numerically (e.g., [8], [9], or [10]) or analytically. In the latter case, the sample has to be approximated by a more or less simplified

model. Depending on the kind of antenna one can use homogeneous cylinders (whole body antennas), homogeneous spheres (head antennas), and the homogeneous half-space (small surface antennas).

At low frequencies, the electromagnetic field can be assumed to be quasi-static and the currents within the sample can be calculated like eddy currents (cf. [11]). Eddy current solutions exist for arbitrary shaped antennas in presence of a lossy sphere [12], an infinite half-space [13], an infinitely long cylinder [14], and an infinitely long elliptical cylinder [15].

In 1985, the optimum radius a^{opt} and the maximum SNR of a loop-shaped coil lying directly on a lossy half-space was derived in [16]

$$\left(\frac{S}{N}\right)^{\max} = 0,2203 \cdot \frac{MV}{\sqrt{kT\Delta f \kappa_L}} \frac{1}{\sqrt{|z|^5}}$$

for

$$a^{\mathrm{opt}} = \frac{|z|}{\sqrt{5}}. \tag{7}$$

In the following years, a lot of work was carried out to calculate the fields of MR antennas at higher frequencies with propagation effects no longer negligible; especially the fields within a lossy cylinder generated by an infinitely long bodycoil [17] and arbitrary shaped coils without ([7] and [18]) and with a surrounding cylindrical shield [19] were presented.

C. Optimization of MR Array Antennas

It is a straightforward approach to combine two or more single MR antennas to an array antenna to achieve a higher SNR compared to a single coil. As in the general case, the resulting noise voltages at the output of the different antennas will be correlated to a certain extent and one has to find the optimum complex weighting factors (magnitude and phase) for signal summation [20] and [21]. If the relative signal strength $|x_i|$ and phase $\arg(x_i)$ and the noise correlation matrix $\boldsymbol{P}$ of the signals at the output of the n antennas $i = 1 \cdots n$ are known, the optimum complex weighting factor w_i for antenna i is given by ([21, eq. (19)])

$$\boldsymbol{W}^{\mathrm{opt}} \propto \boldsymbol{P}^{-1}\boldsymbol{X}^*$$

with

$$\boldsymbol{W} = \begin{bmatrix} w_1 \\ \vdots \\ w_n \end{bmatrix} \quad \text{and} \quad \boldsymbol{X} = \begin{bmatrix} x_1 \\ \vdots \\ x_n \end{bmatrix}. \tag{8}$$

This will lead to the ultimate SNR that can be achieved with an array of discrete antenna elements

$$\left(\frac{S}{N}\right)^{\max} = \frac{\omega MV}{\sqrt{8kT\Delta f}} \sqrt{\boldsymbol{X}^T\boldsymbol{P}^{-1}\boldsymbol{X}^*}. \tag{9}$$

In theory, one can take an infinite number of small loop antennas, calculate the signals and the noise matrix, and sum the infinite number of signals using the optimum weighting factors $\boldsymbol{W}$. This was done for the quasi-static approximation; an infinite number of small loop coils lying directly on a half-space (surface coil) can achieve an 8% higher SNR than a single optimized loop coil ([22] and [23]). For the loops lying directly on a cylinder (human body) the SNR can only be improved by a small margin of 2% in comparison to an optimum conventional bodycoil (calculated by [24] with neglection of the accumulation of surface charges at the body surface). In the following, known calculations will be extended in several ways to account for the following points.

- Nonzero distance between tissue and antenna array.
- Full wave calculation of the electromagnetic fields (no quasi-static approximation).
- Noise from the tissue *and* the antenna itself is considered within the calculation.
- The array consists of *two* different types of dipole antennas: magnetic *and* electric dipoles.

First, we will briefly present analytical expressions for a general surface coil (Fig. 1) and a general bodycoil (Fig. 2). We will show that the problem of optimizing the resulting SNR is equivalent to the problem of matched filtering with respect to nonwhite noise. We will draw new conclusions from the numerical evaluation of the resulting formulas. Finally, we present some examples for adapting the expressions we found to special antenna geometries like the single- and the double-loop coil, the magnetic dipole, and the birdcage coil.

II. Electromagnetic Field and SNR of General MR Antennas

A. General Surface Coil

It is convenient to reduce the case of the general MR surface coil to a simplified model given in Fig. 1 to allow an analytical treatment. While the lossy tissue is modeled by a homogeneous half-space $z < 0$ with electrical parameters ϵ_r, κ and $\mu_r = 1$, the antenna itself is modeled by a planar surface current density $\boldsymbol{K}(\rho, \varphi)$ in the plane $z = h$. In the most general case, the surface current density $\boldsymbol{K}$ may consist of two parts: a source-free part $\boldsymbol{K}^{(1)}$ and a curl-free part $\boldsymbol{K}^{(2)}$.

As a source-free field can be synthesized by a vector potential, we can express $\boldsymbol{K}^{(1)}$ by means of a z-directed vector potential $\boldsymbol{M}^F(\rho, \varphi)$. $\boldsymbol{M}^F$ could be interpreted as a magnetic dipole surface density and is written here as Fourier–Bessel series with coefficients $W_n^{(1)}(p)$, where p and n can be understood as spatial frequencies in $\boldsymbol{e}_\rho$- and $\boldsymbol{e}_\varphi$-direction, respectively

$$\boldsymbol{K}^{(1)}(\rho, \varphi) = \nabla \times \boldsymbol{M}^F(\rho, \varphi)$$

with

$$\boldsymbol{M}^F(\rho, \varphi) = \sum_{n=-\infty}^{\infty} \int_0^{\infty} W_n^{(1)}(p) J_n(p\rho) e^{jn\varphi}\, dp \boldsymbol{e}_z. \tag{10}$$

Note that an adequate number of small loop coils carrying the appropriate currents can approximate the dipole density $\boldsymbol{M}^F$ and thus the current density $\boldsymbol{K}^{(1)}$.

As $\boldsymbol{K}^{(2)}$ is the curl-free part of $\boldsymbol{K}$, it can be derived from a scalar potential, which is also written as a Fourier–Bessel series

$$\boldsymbol{K}^{(2)}(\rho, \varphi) = \sum_{n=-\infty}^{\infty} \int_0^{\infty} W_n^{(2)}(p) \nabla J_n(p\rho) e^{jn\varphi}\, dp. \tag{11}$$

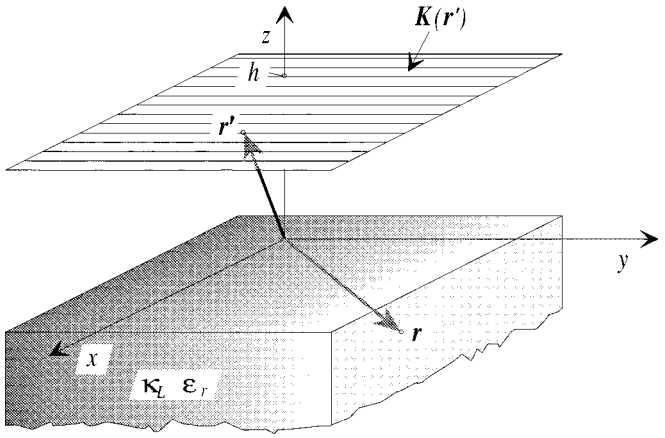

Fig. 1. A planar current density $\boldsymbol{K}(\boldsymbol{r}')$ above a half-space with conductivity κ_L and relative permittivity ϵ_r. The current density is at $z = h$.

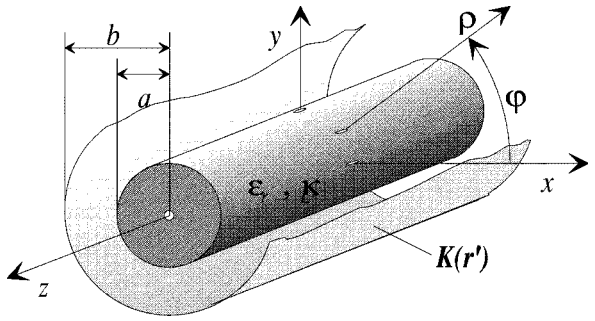

Fig. 2. A cylindrical current density $\boldsymbol{K}(\boldsymbol{r}')$ enclosing a cylinder (radius a) with conductivity κ_L and relative permittivity ϵ_r. The current density is at $\rho = b$.

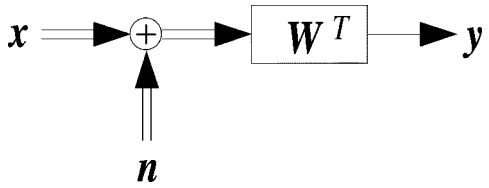

Fig. 3. System theoretical representation of the signal of an MR receiving antenna. Signal $\boldsymbol{x}$ with spectrum $\boldsymbol{X}$ and noise $\boldsymbol{n}$ with power spectrum $\boldsymbol{P}$ are filtered by a filter $\boldsymbol{W}^T$.

Like the polarization current [25, eq. (14)–(71)] $\boldsymbol{K}^{(2)}$ may be seen as result of a electric dipole surface density $\boldsymbol{P}^F$

$$\boldsymbol{K}^{(2)}(\rho, \varphi) = j\omega \boldsymbol{P}^F(\rho, \varphi)$$

with

$$\boldsymbol{P}^F(\rho, \varphi) = \frac{1}{j\omega} \sum_{n=-\infty}^{\infty} \int_0^{\infty} W_n^{(2)}(p) \nabla J_n(p\rho) e^{jn\varphi}\, dp. \tag{12}$$

A sufficient number of small electrical dipoles with an appropriate dipole moment lying in the plane $z = h$ may also be seen as a representation of $\boldsymbol{P}^F$ and thus $\boldsymbol{K}^{(2)}$.

The electromagnetic field from any given current density $\boldsymbol{K}(\rho, \varphi)$ can be calculated using the appropriate dyadic Green's function (DGF) [26, ch. 11]. This method fully includes the influence of the tissue-air boundary, which is often neglected

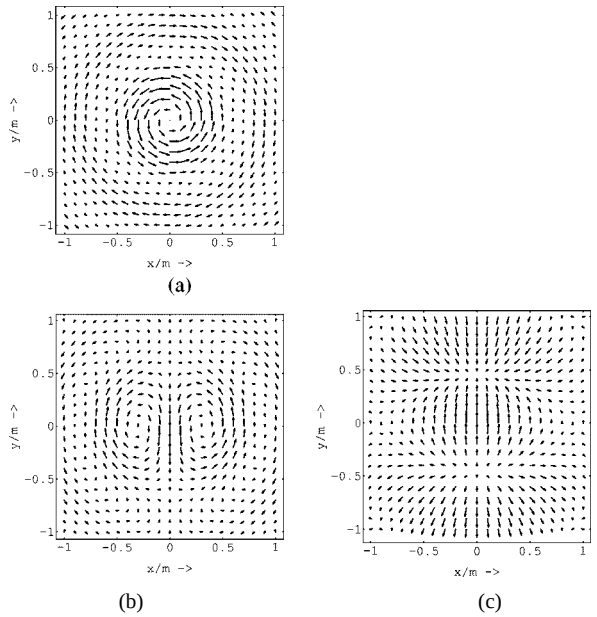

Fig. 4. The current distributions (a) $\boldsymbol{K}_0^{(1)}(p, \rho, \varphi)$, (b) $\boldsymbol{K}_1^{(1)}(p, \rho, \varphi)$ (middle), and (c) $\boldsymbol{K}_1^{(2)}(p, \rho, \varphi)$ for an exemplary $p = 3/\mathrm{m}$.

in quasi-static calculations; ohmic currents within the tissue and perpendicular to the tissue surface lead to a charge accumulation at the tissue–air boundary, which, in return, causes an electrical field. The DGF method also intrinsically accounts for the field generated by the charge accumulation $\sigma = j\omega^{-1}\nabla \boldsymbol{K}$ of the antenna current density $\boldsymbol{K}$ (see Fig. 2. After defining the continuous eigenvalue parameters of air and tissue, respectively

$$\eta(p) = \sqrt{\omega^2 \epsilon_0 \mu_0 - p^2} \tag{13}$$

$$\gamma(p) = \sqrt{\omega^2 \epsilon_0 \epsilon_r \mu_0 - j\omega \mu_0 \kappa_L - p^2} \tag{14}$$

we write the DGF as a Fourier–Bessel series of the vector wave functions [27, eq. (2)-(185)]:

$$\boldsymbol{M}_{\eta, n}^{-}(p, \boldsymbol{r}) = \nabla \times J_n(p\rho) e^{jn\varphi} e^{j\eta z} \boldsymbol{e}_z \tag{15}$$

$$\boldsymbol{N}_{\eta, n}^{-}(p, \boldsymbol{r}) = \frac{1}{k_0} \nabla \times \nabla \times J_n(p\rho) e^{jn\varphi} e^{j\eta z} \boldsymbol{e}_z. \tag{16}$$

We finally end up with the following expressions for the field within the homogeneous half-space:

$$\boldsymbol{E}(\boldsymbol{r}) = -\frac{\omega \mu_0}{4\pi} \sum_{n=-\infty}^{\infty} \int_0^{\infty} \cdot \left\{ \boldsymbol{M}_{\gamma, n}^{-}(p, \boldsymbol{r}) V_n^M(p) + \boldsymbol{N}_{\gamma, n}^{-}(p, \boldsymbol{r}) V_n^N(p) \right\} dp \tag{17}$$

$$\boldsymbol{B}(\boldsymbol{r}) = -j\frac{\mu_0 k}{4\pi} \sum_{n=-\infty}^{\infty} \int_0^{\infty} \cdot \left\{ \boldsymbol{N}_{\gamma, n}^{-}(p, \boldsymbol{r}) V_n^M(p) + \boldsymbol{M}_{\gamma, n}^{-}(p, \boldsymbol{r}) V_n^N(p) \right\} dp \tag{18}$$

where the weighting coefficients $V^{M,N}$ of the vector wave functions are derived from the Fourier–Bessel coefficients $W^{(1,2)}$ of the current density $\boldsymbol{K}$ multiplied with a transformation matrix $\boldsymbol{T}(h)$

$$\begin{bmatrix} V_n^M(p) \\ V_n^N(p) \end{bmatrix} = \boldsymbol{V} = \boldsymbol{T}^T \boldsymbol{W} = \begin{bmatrix} \frac{4\pi}{\eta+\gamma} e^{-j\eta h} & 0 \\ 0 & -j\frac{4\pi\eta k}{\eta k^2+\gamma k_0^2} e^{-j\eta h} \end{bmatrix} \cdot \begin{bmatrix} W_n^{(1)}(p) \\ W_n^{(2)}(p) \end{bmatrix}. \tag{19}$$

Assuming a y-directed static magnetic field B_0, the magnetization $\boldsymbol{M}$ at the point $\boldsymbol{r}$ may be written as

$$\boldsymbol{M} = \sqrt{2}M(\boldsymbol{e}_x - j\boldsymbol{e}_z) \tag{20}$$

where the factor $\sqrt{2}$ accounts for the fact that M is usually understood as a root mean square (rms) value (e.g., [23]). If we choose the point of interest $\boldsymbol{r}$ lying directly on the $\boldsymbol{z}$-axis within the tissue (i.e., $\boldsymbol{r} = (0,\, 0,\, z < 0)$) we derive the following scalar product:

$$\boldsymbol{M} \cdot \boldsymbol{B}(0,\, 0,\, z) = \sqrt{2}M \sum_{n=-\infty}^{\infty} \int_0^{\infty} \boldsymbol{W}^T \boldsymbol{T} \boldsymbol{S}\, dp \tag{21}$$

with

$$\boldsymbol{S} = \frac{\mu_0}{4\pi} \begin{bmatrix} \frac{\gamma p}{2}(\delta_{n-1} - \delta_{n+1}) - p^2\delta_n \\ \frac{kp}{2}(\delta_{n-1} + \delta_{n+1}) \end{bmatrix} e^{j\gamma z} \tag{22}$$

and

$$\delta_n = \begin{cases} 1, & \text{for } n = 0 \\ 0, & \text{else} \end{cases}$$

which represents the signal strength in (4). On the other hand, the losses within the tissue P_L may be calculated by (6) and (17) applying the Parseval theorem (cf. [28, eqs. (3.13b), (4.42)]) and the orthogonality relation for Bessel functions (cf. [27, eq. (173d)]). We finally end up with

$$P_L = \sum_{n=-\infty}^{\infty} \int_0^{\infty} \boldsymbol{W}^T \boldsymbol{T} \boldsymbol{P}_L \boldsymbol{T}^{T*} \boldsymbol{W}^* \, dp \tag{23}$$

with

$$\boldsymbol{P}_L = \frac{(\omega\mu_0)^2 \kappa_L}{16\pi \cdot j(\gamma - \gamma^*)} \begin{bmatrix} p & 0 \\ 0 & \frac{p}{kk^*}(\gamma\gamma^* + p^2) \end{bmatrix}. \tag{24}$$

In a similar fashion the losses within the planar antenna itself can be written [cf. (5)]

$$P_A = \sum_{n=-\infty}^{\infty} \int_0^{\infty} \boldsymbol{W}^T \boldsymbol{P}_A \boldsymbol{W}^* \, dp \tag{25}$$

with

$$\boldsymbol{P}_A = \frac{\pi}{\kappa_A d} \begin{bmatrix} p & 0 \\ 0 & p \end{bmatrix} = \frac{\pi p}{\kappa_A d} \boldsymbol{I} \tag{26}$$

with $\boldsymbol{I}$ being the unity matrix. Putting all together the SNR of a general surface coil with weighting coefficents $\boldsymbol{W}$ may be expressed in this extremely compact form [cf. (4)]

$$\left(\frac{S}{N}\right)(\boldsymbol{r}) = \frac{\omega M V \left| \sum_{n=-\infty}^{\infty} \int_0^{\infty} \boldsymbol{W}^T \boldsymbol{X}\, dp \right|}{\sqrt{8kT\Delta f \sum_{n=-\infty}^{\infty} \int_0^{\infty} \boldsymbol{W}^T \boldsymbol{P} \boldsymbol{W}^*\, dp}} \tag{27}$$

with

$$\boldsymbol{X} = \boldsymbol{T}\boldsymbol{S}$$

and

$$\boldsymbol{P} = \boldsymbol{T}\boldsymbol{P}_L\boldsymbol{T}^{T*} + \boldsymbol{P}_A.$$

B. General Bodycoil

Like the general surface coil, the general bodycoil has also to be composed of two parts expressed by a double Fourier series; a source-free part

$$K^{(1)}(\varphi,\, z) = \sum \int W_n^{(1)}(m) \nabla \times e^{jn\varphi} e^{jmz} \boldsymbol{e}_\rho \, dm \tag{28}$$

which is caused by a ϱ-oriented magnetic dipole density and a curl-free part

$$K^{(2)}(\varphi,\, z) = \sum \int W_n^{(2)}(m) \nabla e^{jn\varphi} e^{jmz} \, dm \tag{29}$$

which is caused by a electric dipole density lying in the $\varrho = b$-plane. Here, m and n represent spatial frequencies in $\boldsymbol{e}_z$- and $\boldsymbol{e}_\varphi$-direction, respectively. The appropriate DGF of this problem is composed of a double Fourier series of slightly different vector wave functions (cf. [26, ch. 7])

$$\boldsymbol{M}_{\eta,\,n}(m,\, \boldsymbol{r}) = \nabla \times J_n(\eta\rho) e^{jn\varphi} e^{jmz} \boldsymbol{e}_z \tag{30}$$

$$\boldsymbol{N}_{\eta,\,n}(m,\, \boldsymbol{r}) = \frac{1}{k_0} \nabla \times \nabla \times J_n(\eta\rho) e^{jn\varphi} e^{jmz} \boldsymbol{e}_z \tag{31}$$

which leads to the electromagnetic field within the conductive tissue

$$\boldsymbol{E}(\boldsymbol{r}) = -\frac{\omega\mu_0}{8\pi} \sum_{n=-\infty}^{\infty} \int_{-\infty}^{\infty} \cdot \left\{ \boldsymbol{M}_{\gamma,\,n}(m,\, \boldsymbol{r}) V_n^M(m) + \boldsymbol{N}_{\gamma,\,n}(m,\, \boldsymbol{r}) V_n^N(m) \right\} dm \tag{32}$$

$$\boldsymbol{B}(\boldsymbol{r}) = -j\frac{\mu_0 k}{8\pi} \sum_{n=-\infty}^{\infty} \int_{-\infty}^{\infty} \cdot \left\{ \boldsymbol{N}_{\gamma,\,n}(m,\, \boldsymbol{r}) V_n^M(m) + \boldsymbol{M}_{\gamma,\,n}(m,\, \boldsymbol{r}) V_n^N(m) \right\} dm \tag{33}$$

where the weighting coefficients $V^{M,N}$ of the vector wave functions are derived from the Fourier coefficients $W^{(1,2)}$ of

the current density $\boldsymbol{K}$ by $\boldsymbol{V} = \boldsymbol{T}^T\boldsymbol{W}$ with the transformation matrix

$$\boldsymbol{T}^T = -j\frac{4\pi^2 b}{\eta^2}\left\{H_n^{(2)'}(\eta b)\begin{bmatrix} e_n(m) \\ f_n(m)\end{bmatrix}\begin{bmatrix}\eta m \\ \dfrac{\eta n}{b}\end{bmatrix} + H_n^{(2)}(\eta b)\begin{bmatrix} g_n(m) \\ h_n(m)\end{bmatrix}\begin{bmatrix}\dfrac{nk_0}{b} \\ \dfrac{m}{k_0}\left[\left(\dfrac{n}{b}\right)^2 - \eta^2\right]\end{bmatrix}\right\}. \quad (34)$$

The functions $e_n(m)\cdots h_n(m)$ are coefficients to fulfill the boundary conditions at the $\varrho = a$-plane and can be found elsewhere ([26, ch. 7] or [19]).

Here, we assume a z-directed B_0-field, which means that the magnetization $\boldsymbol{M}$ must be written as

$$\boldsymbol{M} = \sqrt{2}M(\boldsymbol{e}_x + j\boldsymbol{e}_y). \quad (35)$$

So the calculation of the SNR of the general bodycoil becomes very similar to the case of the general surface coil. After a lengthy calculation, we end up with (27) and a different integration range $m = -\infty\cdots\infty$. $\boldsymbol{S}$, $\boldsymbol{P}_L$, and $\boldsymbol{P}_A$ are given by

$$\boldsymbol{S} = \frac{\mu_0\gamma}{8\pi}\begin{bmatrix}-m \\ k\end{bmatrix}J_{n+1}(\gamma\rho) \quad (36)$$

$$\boldsymbol{P}_L = \frac{\kappa_L}{2}\left(\frac{\omega\mu_0}{4}\right)^2\frac{\gamma\gamma^*}{2} \cdot \begin{bmatrix} F_{n-1}+F_{n+1} & \dfrac{m}{k^*}[F_{n-1}-F_{n+1}] \\ \dfrac{m}{k}[F_{n-1}-F_{n+1}] & \dfrac{m^2}{kk^*}\left[F_{n-1}+F_{n+1}+2\dfrac{\gamma\gamma^*}{m^2}F_n\right]\end{bmatrix} \quad (37)$$

with

$$F_n(\gamma, a) = \int_0^a J_n(\gamma\rho)J_n(\gamma^*\rho)\rho\,d\rho \quad (38)$$

and

$$\boldsymbol{P}_A = \frac{2\pi^2}{\kappa_A d}\left[m^2 + \left(\frac{n}{b}\right)^2\right]\boldsymbol{I}. \quad (39)$$

Note that the noise correlation matrix P_L also has elements outside the main diagonal. This means that the noise contributions of the different vector wave functions $\boldsymbol{M}$ and $\boldsymbol{N}$ are mutually dependent.

III. Ultimate SNR of a General MR Antenna

A. Optimization by Means of the Matched-Filter Theory

Equation (27) is equivalent to filtering the sum of a two-dimensional (2-D) signal $\boldsymbol{x}$ (with spectrum $\boldsymbol{X}$) and a 2-D correlated noise source $\boldsymbol{n}$ (with power spectrum $\boldsymbol{P}$) by a filter $\boldsymbol{W}^T$ (Fig. 3). This implies that the optimization of the SNR can be conducted by means of the matched-filter theory for nonwhite noise, e.g., [29, ch. 5]. The following multidimensional extension of the theory is easy to prove:

$$\boldsymbol{W}_n^{\text{opt}}(p) \sim [\boldsymbol{P}_n^*(p)]^{-1}\boldsymbol{X}_n^*(p) \quad (40)$$

$$\Longrightarrow$$

$$\left(\frac{S}{N}\right)^{\max} = \frac{\omega MV}{\sqrt{8kT\Delta f}} \cdot \sqrt{\sum_{n=-\infty}^{\infty}\int_0^{\infty}\boldsymbol{X}_n^T(p)\left(\boldsymbol{P}_n^{-1}(p)\right)^T\boldsymbol{X}_n^*(p)\,dp}. \quad (41)$$

In the case of a cylindrical receiving antenna, the spatial frequency p must be written as m. Equations (40) and (41) allow us to find the optimum Fourier coefficients $\boldsymbol{W}^{\text{opt}}$ of the current distribution $\boldsymbol{K}$, which a planar or a cylindrical receiving antenna must have to gain the maximum SNR physically possible.

B. Results for the General Surface Coil

Introducing (22), (24), and (26) into the two above expressions leads to the optimum weighting of a planar antenna. Due to the nature of the signal spectrum of the general surface coil (22) the optimum current distribution must be synthesized by a summation of orthogonal current patterns as follows.

- $\boldsymbol{K}_0^{(1)}(p, \rho, \varphi) = \nabla \times J_0(p\rho)\boldsymbol{e}_z$: a rotational symmetric magnetic dipole density detecting a z-oriented $\boldsymbol{B}$-field.
- $\boldsymbol{K}_1^{(1)}(p, \rho, \varphi) = 2\,\nabla \times J_1(p\rho)\cos\varphi\boldsymbol{e}_z$: a magnetic dipole density with a $\sin\varphi$ dependency detecting an x-oriented $\boldsymbol{B}$-field.
- $\boldsymbol{K}_1^{(2)}(p, \rho, \varphi) = 2j\nabla J_1(p\rho)\sin\varphi$: an electric dipole density with a $\sin\varphi$ dependency also detecting a x-oriented $\boldsymbol{B}$-field, weighted with the optimum spectral distributions $W_0^{(1),\,\text{opt}}(p)$, $W_1^{(1),\,\text{opt}}(p)$, and $W_1^{(2),\,\text{opt}}(p)$ depending on frequency, distance between the antenna and the tissue and electrical parameter of the tissue. In Fig. 4, three exemplary orthogonal current patterns contributing to the optimum solution are shown.

Assuming the tissue to be homogeneous muscle tissue (for electrical parameters see [30]) and the magnetization to be frequency independent, we did a numerical evaluation of the maximum SNR for different coil-tissue distances with respect to the frequency. It turned out that a optimum receiver antenna made of copper is nearly as good as a lossless antenna if the frequency is higher than approximately 20 MHz and the coil-tissue distance is small (Fig. 5). With increasing coil-tissue distance h, the spectral distribution $\boldsymbol{W}_{0,1}(p)$ of the optimum current distribution grows at higher frequencies. That means that the structural size of the current distribution $\boldsymbol{K}^{\text{opt}}$ decreases with increasing distance h (Fig. 6). For $h > |z|$, the optimum spectrum $\boldsymbol{W}(p)$ becomes divergent for $p \to \infty$. In this case, an optimum $\boldsymbol{K}(\rho, \varphi)$ no longer exists.

C. Results for the General Bodycoil

Using (36)–(39) and (40), a body antenna that achieves an optimum SNR in any point of interest $\boldsymbol{r}$ within the tissue can be found. But as bodycoils are commonly used to image the central region of the human body, it is of practical interest to restrict $\boldsymbol{r}$ to the z-axis (i.e., $\rho = 0$). In this case, all weighting coefficients $\boldsymbol{W}_n^{\text{opt}}(p)$ vanish except for $n = -1$ as can be seen from (36). This results in a cylindrical current distribution $\boldsymbol{K}^{\text{opt}}(\varphi, z)$, which has a $e^{j\varphi}$-dependency for the φ-direction.

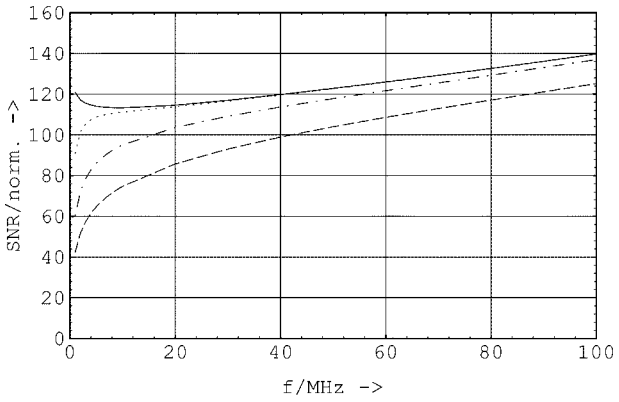

Fig. 5. SNR of a copper antenna optimized for $\boldsymbol{r} = (0,\ 0,\ -10$ cm) with a different coil-tissue distance h: $\cdots$ $h = 0$; $\cdot$ - $\cdot$ - $h = 5$ cm; and - - - $h = 10$ cm. For comparison, maximum SNR of a lossless antenna (—).

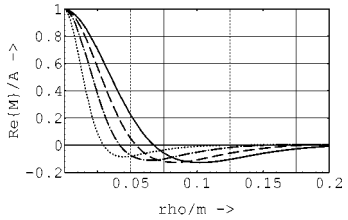

Fig. 6. Real part of the rotational symmetric contribution of the optimized magnetic dipole distribution $\boldsymbol{M}^F$. The antenna ($f = 100$ MHz) is optimized for $z = -10$ cm and has different coil-tissue distances h: — 0 cm; - - - 2 cm; $\cdot$ - $\cdot$ - 4 cm; and $\cdots$ 6 cm.

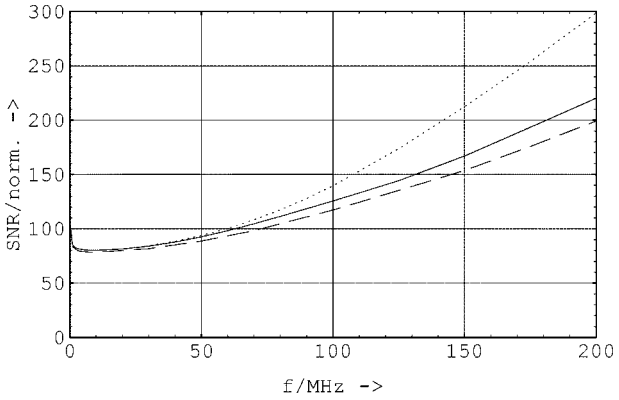

Fig. 7. SNR of a lossless body coil solely built of magnetic dipoles and optimized for a point on the z-axis: $b = a = 20$ cm (—) and $b = 30$ cm (- - -). For comparison, an antenna built of magnetic *and* electric dipoles ($\cdots$).

As the human body is more or less inhomogeneous we have to compute with "effective" electrical tissue parameters for the homogeneous cylinder model. We scaled the parameters of muscle tissue ([30]) to get the effective parameters found by [31]. From the numerical evaluation (Fig. 7) we see that electric dipoles do not play an important role within the optimum current distribution as long as the antenna is close to the surface of the tissue and the frequency is below 100 MHz. Similar to the optimum surface antenna, the structural size of the optimum cylindrical current distribution decreases with increasing ratio of antenna radius b to body radius a (Fig. 8).

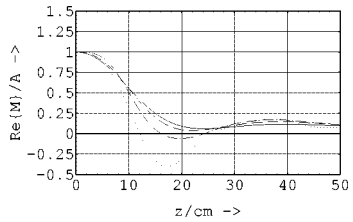

Fig. 8. Real part of the magnetization $\boldsymbol{M}^F$ of a cylindrical lossless antenna that is optimized for the coordinate origin $\boldsymbol{r} = (0,\ 0,\ 0)$. The results are plotted for a fixed load radius $a = 20$ cm and four different antenna radii b ($f = 100$ MHz): 20 cm (—); 22.5 cm (- -); 25 cm ($\cdot$ - $\cdot$ -); and 27.5 cm ($\cdots$).

IV. Application to Special Cases

A. Loop Coils

1) The Conventional Loop Coil: In its simplest design a surface antenna is just a loop coil (radius a) made of copper wire (wire radius R, see Fig. 9). Assuming a zero coil-tissue distance h and quasi-static conditions the optimium coil radius a^{opt} of a lossless coil was found by [16]: (7). The frequency dependency was partly analyzed by [32]. In [33] it was shown that lossy coils must have a bigger coil radius a^{opt} than lossless coils. All effects can easily be studied with the formulas we found if we apply the appropriate weighting function of a circular line current

$$W_0^{(1),\,\text{loop}}(p) = IaJ_1(pa). \tag{42}$$

All other coefficients must be set to zero. Calculating the coil losses we have considered two possibilities.

1) The wire radius R is independent of the loop radius a. The losses are proportional to a

$$P_A = \frac{a}{\kappa_A R\delta}\, I^2 \sim a. \tag{43}$$

2) The wire radius R is scaled like the coil radius a: $R = \beta a$. Thus, the antenna losses are independent of a

$$P_A = \frac{a}{\kappa_A R\delta}\, I^2 = \frac{I^2}{\kappa_A \beta\delta}. \tag{44}$$

Finally, we found the following expression containing integrals without an analytical solution as shown in (45), at the bottom of the next page. A numerical optimization of a (Fig. 10) shows a theoretical verification of an effect found by [33]; lossy coils must have a bigger coil radius a^{opt} than lossless coils. Whereas a lossless coil would have a vanishing coil radius a^{opt} for a coil-tissue distance h bigger than a certain value depending on the depth of the point of interest and on frequency, the radius a of a lossy coil increases again for large distances h. This trend reversal is due to the fact that the coil losses become dominant of the tissue losses with increasing h.

2) Small Magnetic Dipole Antenna: In [34] it was suggested to use a loop coil with a vanishing radius $a \to 0$ and to optimize its distance h to the tissue. The quasi-static calculation showed that this magnetic dipole is best placed at $h^{\text{opt}} = 0.2|z|$. If we

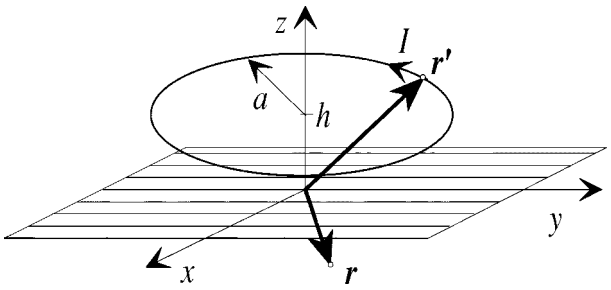

Fig. 9. A circular line current $\boldsymbol{I}$ with radius a and distance h to the tissue.

keep in mind the relation $\lim_{a\to 0} J_1(pa)/a = 0.5p$, we can easily calculate the optimum distance for any given frequency with (45), as shown in (46) at the bottom of the page. Obviously, a coil made of material with a finite conductivity κ will have infinite losses when its radius approaches zero. The numerical optimization (Fig. 11) shows that even a relatively large dipole coil (coil radius $a = 1$ cm and wire radius $R = 1$ mm resulting in $\beta = 0.1$) has a much smaller SNR than a superconducting dipole of same size. A lossless dipole coil at $f = 64$ MHz has an SNR of 75, which is only slightly less than the SNR of 79 of a lossless loop coil with optimum radius and tissue distance (Fig. 10).

3) Dual-Loop Coil: In 1996, a dual-loop coil configuration was presented in [35]. The two loop coils with radius a lie in the same x–y-plane. They carry a current with the same magnitude I but with a phase difference of 2φ, and have a center-to-center distance of $2b$. As the expressions shown were only valid for quasi-static conditions and a zero antenna–tissue distance, we wanted to overcome these restrictions by extending our expressions for the field of a simple loop coil. Doing so we converted (17)–(19) into Cartesic coordinates by a Hankel–Fourier transformation to find more suitable expressions for the proposed

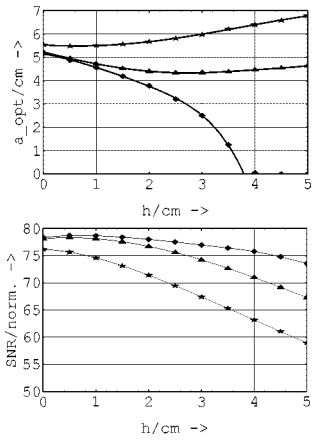

Fig. 10. a^{opt} and $(S/N)^{\max}$ for a 10-cm-deep point of interest and for different coil-tissue distances h at $f = 64$ MHz. The parameter is $\beta = R/a$: ♦ lossless coil; ▲ copper with $\beta = 0.1$; and ★ copper with $\beta = 0.01$.

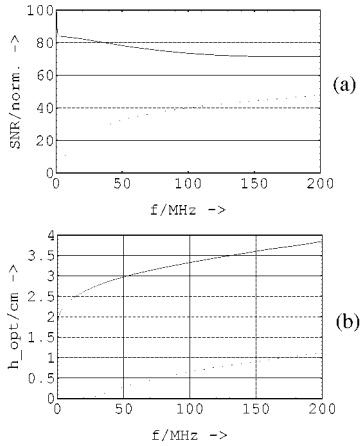

Fig. 11. (a) Maximum SNR of a small loop coil ($a = 1$ cm, $\beta = 0.1$, and $z = 10$ cm and (b) optimum distance h^{opt} to the tissue. — lossless antenna material, and - - - copper coil.

$$\left(\frac{S}{N}\right)(\boldsymbol{r}) = \frac{\omega MV|\boldsymbol{B}(\boldsymbol{r})\cdot(\boldsymbol{e}_x - j\boldsymbol{e}_z)|}{\sqrt{8kT\Delta f\,(P_A+P_L)}} = \frac{MV}{\sqrt{kT\Delta f}}\cdot\frac{\left|\int_0^\infty \frac{p^2}{\eta+\gamma}\,J_1(pa)e^{j(\gamma z-\eta h)}\,dp\right|}{\sqrt{\frac{8}{\omega^2\mu_0^2\kappa_A R\delta a}+8\pi\kappa_L\int_0^\infty \frac{J_1^2(pa)}{|\eta+\gamma|^2}\,\frac{p}{j(\gamma-\gamma^*)}\,e^{j(\eta^*-\eta)h}\,dp}} \tag{45}$$

$$\left(\frac{S}{N}\right)_{a=0} = \frac{MV}{\sqrt{kT\Delta f}}\cdot\frac{\left|\int \frac{p^3}{\eta+\gamma}\,e^{j(\gamma z-\eta h)}\,dp\right|}{\sqrt{\lim_{a\to 0}\frac{32}{\omega^2\mu_0^2\kappa_A\beta\delta a^4}+8\pi\kappa_L\int \frac{e^{j(\eta^*-\eta)h}}{|\eta+\gamma|^2}\,\frac{p^3}{j(\gamma-\gamma^*)}\,dp}} \tag{46}$$

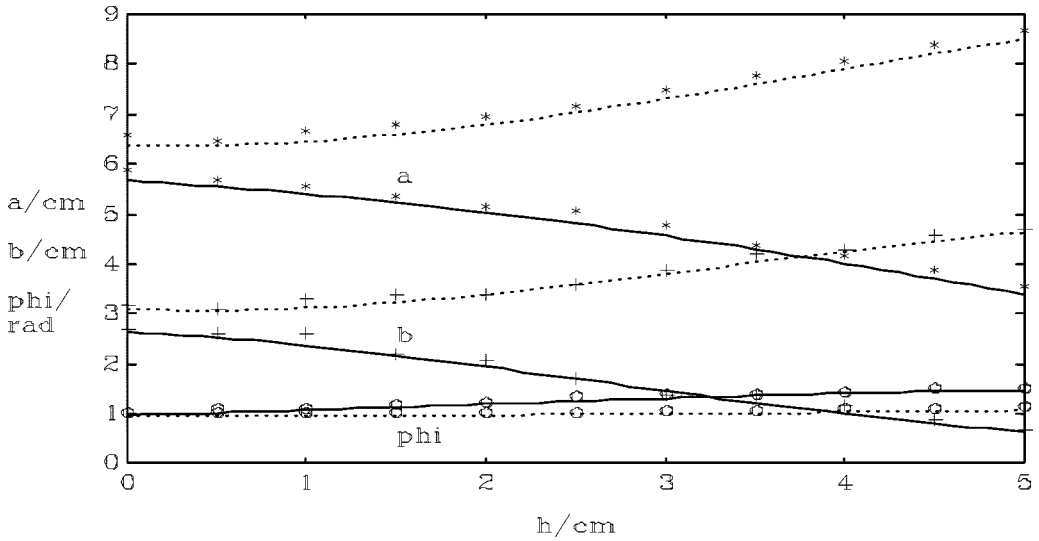

Fig. 12. Optimum parameters a^{opt} (⋆), b^{opt} (+), φ^{opt} (∘) for maximized SNR of the point $(0,\ 0,\ -10\ \mathrm{cm})$ as a function of h for $f = 64$ MHz. Comparison of lossless coils (–) with lossy copper coils with wire radius $R = 0.005a$ (- -), both at 64 MHz.

dual-coil problem (shown in [36], with $p^2 = u^2 + v^2$ and $F(p) = J_1(pa)e^{-j\eta h}/(\eta+\gamma)$)

$$\boldsymbol{E}_{\mathrm{single}}(x,\ y,\ z<0) = \frac{\omega\mu_0 Ia}{2\pi}\iint \begin{bmatrix} vx \\ -uy \\ 0 \end{bmatrix} \frac{F(p)}{p}\, e^{j(ux+vy+\gamma z)}\, du\, dv \quad (47)$$

$$\boldsymbol{B}_{\mathrm{single}}(x,\ y,\ z<0) = \frac{\mu_0 Ia}{2\pi}\iint \begin{bmatrix} -u\gamma \\ -v\gamma \\ p^2 \end{bmatrix} \frac{F(p)}{p}\, e^{j(ux+vy+\gamma z)}\, du\, dv. \quad (48)$$

Now the electromagnetic field of the dual-surface coil can easily be derived from a superposition of the fields of two single-loop coils with a translation of $\pm b$ on the y-axis

$$\boldsymbol{E}_{\mathrm{dual}}\left(\begin{bmatrix} x \\ y \\ z<0 \end{bmatrix}\right) = e^{-j\varphi}\boldsymbol{E}_{\mathrm{single}}\left(\begin{bmatrix} x \\ y-b \\ z \end{bmatrix}\right) + e^{j\varphi}\boldsymbol{E}_{\mathrm{single}}\left(\begin{bmatrix} x \\ y+b \\ z \end{bmatrix}\right). \quad (49)$$

We arrive at

$$\boldsymbol{B} = -j\frac{\mu_0 Ia}{2\pi}\iint \begin{bmatrix} 0 \\ \gamma v \sin vb \sin\varphi \\ p^2 \cos vb \cos\varphi \end{bmatrix} \frac{F(p)}{p}\, e^{j\gamma z}\, du\, dv \quad (50)$$

for the $\boldsymbol{B}$-field at the point of interest $(0,\ 0,\ z<0)$ and at

$$P_L = \frac{\kappa_L}{2}\int_V \boldsymbol{E}\cdot\boldsymbol{E}^*\, dV = 2\kappa_L(Ia\omega\mu_0)^2\pi \iint \frac{\cos^2(vb-\varphi)}{j(\gamma-\gamma^*)}\,|F(p)|^2\, du\, dv \quad (51)$$

for the losses within the lower half-space. If we assume the radius R of the wire scaling with the radius a of the loop ($R = \beta a$), we can calculate the ohmic losses of the two loop antennas by $P_A = 2I^2/(\kappa_A\beta\delta)$, where δ is the skin depth of the wire material (κ_A). Introducing the above expressions into (4) gives us the SNR of the dual-loop coil, which can only numerically be maximized as in the case of the single loop coil and the dipole coil.

We calculated the optimum parameters (Fig. 12) for the maximum SNR of a point 10 cm below the tissue surface ($f = 64$ MHz). A comparison of lossless coils with copper coils ($\beta = R/a = 0.005$) shows a behavior like the single loop coil: while a^{opt} and b^{opt} of the *lossless* dual-loop coil decrease with increasing distance h to the tissue, a^{opt}, and b^{opt} of the *lossy* dual-loop coil increase. For $f = 64$ MHz and $h = 0$ cm the lossless dual-loop coil achieves a 22% SNR gain over the optimized single-loop coil (19% for copper, single loop with $\beta = R/a = 0.01$, dual loop with $\beta = 0.005$).

B. Birdcage Resonator

The so-called "birdcage" resonator (introduced by Hayes *et al.*[37]) is a special kind of body resonator that can ideally be represented by a sourceless cylindrical current density [cf. [24, eq. (1)]]

$$\boldsymbol{K}_{bc}(\varphi,\ z) = \nabla\times\boldsymbol{M}^F_{bc}(\varphi,\ z), \qquad \text{with} \quad (52)$$

$$\boldsymbol{M}^F_{bc}(\varphi,\ z) = \begin{cases} \hat{M}^F_{bc}e^{-j\varphi}\boldsymbol{e}_\rho, & -c\le z\le c \\ 0, & \text{otherwise} \end{cases} \quad (53)$$

on a cylinder surface with radius b: Fig. 13. It is easy to show that an unloaded birdcage resonator with $c\to\infty$ (i.e., only z-directed currents) has a completely homogeneous circular $\boldsymbol{B}$-field for all points surrounded by the antenna (i.e., $\varrho < b$). Choosing just the real part $\mathrm{Re}\{\boldsymbol{K}_{bc}\}$ of (53) gives us an antenna with a linearly polarized field (x-direction). To maximize the SNR in the center, the length $2c$ of the resonator has to be optimized with respect to the radii a and b. In [24], this was done under the quasi-static assumption: with $b = a$ a birdcage resonator with optimized length $2c^{\mathrm{opt}} \approx 0.8a$ gains 98% of the maximum SNR physically possible. To get a design rule for higher frequencies, we can use the found expressions for the SNR of a general body

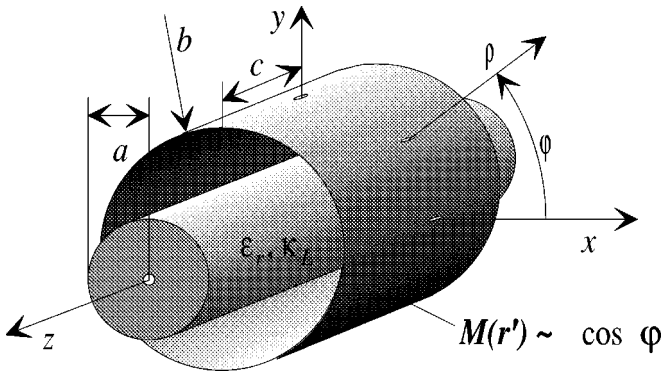

Fig. 13. The "birdcage" resonator may be modeled by a cylindrical magnetization with length $2c$ and a sinusoidal dependency in φ-direction.

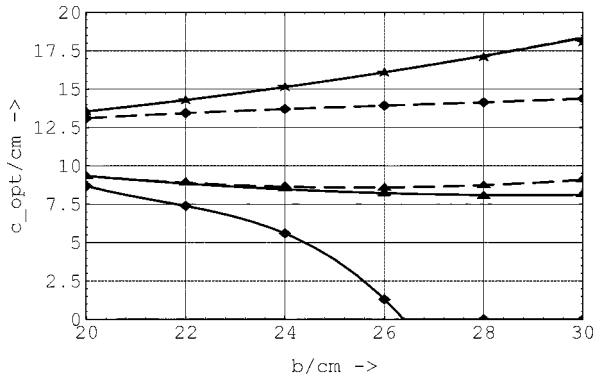

Fig. 14. Optimum half length c^{opt} of a birdcage resonator at the frequencies $f = 1$ MHz (♦), 50 MHz (▲), and 100 MHz (★). The resonator is either lossless (—) or made of copper (- - -). The antenna has the same radius b as the cylindrical tissue a: $b = a = 20$ cm. Note that there is no visible difference between the lossless and the lossy resonator at $f = 100$ MHz as the tissue losses dominate the coil losses by far at this frequency.

coil by applying the appropriate Fourier coefficients for the birdcage coil

$$W^{(1)}_{n,bc}(m,\, c) = \frac{1}{2\pi}\, \mathcal{F}_{\varphi,z}\{\boldsymbol{M}^F_{bc}(\varphi,\, z)\cdot \boldsymbol{e}_\rho\} = \frac{\hat{M}^F_{bc}}{\pi}\, \frac{\sin(mc)}{m}\, \delta_{n+1} \tag{54}$$

and $W^{(2)}_{n,bc}(m,\, c) = 0$. Similar to the optimum radius a^{opt} of a lossy loop coil (Fig. 10), the optimum length $2c^{\mathrm{opt}}$ of a lossy birdcage resonator always has to be larger than the optimum size of a lossless antenna: Fig. 14. This effect is easy to see for conditions where the coil losses become dominant of the tissue losses: at a low frequency f or for a large antenna–tissue distance $b-a$. But opposed to a^{opt} of a lossless loop coil, $2c^{\mathrm{opt}}$ of a lossless birdcage becomes zero only for low frequencies if the distance to the tissue is increased.

V. Discussion

From the presented results we come to the following conclusions.

1) The quasi-static assumption for the field calculation of MR antennas is only valid up to $f = 30 \cdots 40$ MHz.
2) The SNR of an optimized *lossless* antenna is independent of the distance to the tissue as long as the coil-tissue distance is smaller than the depth of the point of interest within the tissue.
3) At higher frequencies an antenna array synthesized by magnetic dipoles perpendicular to the tissue surface cannot reach the maximum SNR physically possible. To reach the limit a second kind of dipoles has to be employed for synthesizing the MR array antenna: here we suggested using electric dipoles parallel to the tissue surface, but magnetic dipoles parallel to the tissue surface could equivalently be used.
4) Convenient MR antennas (loop coil, birdcage) nearly reach the physical SNR limit under the following conditions: low frequency, low intrinsic antenna losses, small distance to the tissue, and optimum size of the antenna. With these constraints a loop coil can reach 90% of the maximum SNR up to a frequency $f = 50$ MHz, a birdcage even up to $f = 70$ MHz.

Detecting an NMR signal with the maximum SNR physically possible requires an antenna current distribution which is unlimited in the spatial frequency space (discrete spatial frequency n and continuous spatial frequencies m and p, respectively). A technical realization of the optimum antenna will only account for the spatial frequencies up to a certain limit. Therefore the tradeoff between these "spatial cutoff frequencies" and the gained SNR is of particular interest. Different spatial lowpass filterings could be treated using the presented formula to find the optimum relation between SNR and the costly technical effort for the MR receiving antenna.

References

[1] F. Bloch, W. W. Hansen, and M. Packard, "Nuclear induction," *Phys. Rev.*, vol. 69, p. 127, 1946.
[2] E. M. Purcell, H. C. Torrey, and R. V. Pound, "Resonance absorption by nuclear magnetic moments in a solid," *Phys. Rev.*, vol. 69, pp. 37–38, 1946.
[3] P. C. Lauterbur, "Image formation by induced local interactions: Examples employing nuclear magnetic resonance," *Nature*, vol. 242, pp. 190–191, 1973.
[4] A. Kumar, D. Welti, and R. R. Ernst, "NMR Fourier zeugmatography," *J. Magn. Res.*, vol. 18, pp. 69–83, 1975.
[5] D. I. Hoult and R. E. Richards, "The signal-to-noise ratio of the nuclear magnetic resonance experiment," *J. Magn. Res.*, vol. 24, pp. 71–85, 1976.
[6] D. I. Hoult and P. C. Lauterbur, "The sensitivity of the zeugmatographic experiment involving human samples," *J. Magn. Res.*, vol. 34, pp. 425–433, 1979.
[7] H. Vesselle and R. E. Collin, "The signal-to-noise ratios of nuclear magnetic resonance surface coils and application to a lossy dielectric cylinder model—Part I: Theory," *IEEE Trans. Biomed. Eng.*, vol. 42, pp. 497–506, May 1995.
[8] W. Dürr, "Three-dimensional electromagnetic field calculation of MR-antennas," in *Proc. 7th Annu. Meet. Soc. Magn. Res. Med.*, San Francisco, CA, Aug. 1988, p. 844.
[9] W. Renz, W. Dürr, and R. Oppelt, "A reduced size body resonator for fast imaging techniques," in *Proc. 2nd Annu. Meet. Annu. Meet. Soc. Magn. Res. Med.*, San Francisco, CA, Aug. 1994, p. 1112.
[10] H. Ochi and E. Yamamoto, "Analysis of a magnetic resonance imaging antenna inside an RF-shield," *Elect. Commun. Japan*, pt. 1, vol. 77, no. 1, pp. 37–45, 1994.

[11] J. A. Tegopoulos and E. E. Kriezis, *Eddy Currents in Linear Conducting Media*. Amsterdam, The Netherlands: Elsevier, 1985.
[12] L. Hannakam, "Wirbelströme in der Kugel bei beliebig geformter erregender Leiterschleife," *Zeitschr. angew. Physik*, vol. 32, no. 5/6, pp. 348–355, 1972.
[13] ——, "Wirbelströme im leitenden Halbraum bei beliebiger Form der erregenden Leiterschleife," *Archiv Elektrotechnik*, vol. 54, no. 5, pp. 251–261, 1972.
[14] ——, "Wirbelströme in einem massiven Zylinder," *Archiv Elektrotechnik*, vol. 55, no. 4, pp. 207–215, 1973.
[15] M. Filtz, "Über transversale, longitudinale und dreidimensionale Wirbelströme in zylindrischen Leitern mit elliptischen Querschnitt," Ph.D. dissertation, Tech. Universität, Berlin, Germany, 1989.
[16] W. A. Edelstein, T. H. Foster, and J. F. Schenck, "The relative sensitivity of surface coils to deep lying tissues," in *Proc. 4th Annu. Meet. Soc. Magn. Res. Med.*, London, U.K., Aug. 1995, p. 964.
[17] T. K. F. Foo, C. E. Hayes, and Y.-W. Kang, "An analytical model for the design of RF resonators for MR body imaging," *Magn. Res. Med.*, vol. 21, no. 2, pp. 165–177, 1991.
[18] H. Vesselle and R. E. Collin, "The signal-to-noise ratio of nuclear magnetic resonance surface coils and application to a lossy dielectric cylinder model—Part II: The case of cylindrical window coils," *IEEE Trans. Biomed. Eng.*, vol. 42, pp. 507–520, May 1985.
[19] Q. Chen, K. Sawaya, T. Uno, S. Adachi, H. Ochi, and E. Yamamoto, "A three-dimensional analysis of slotted tube resonator for MRI," *IEEE Trans. Med. Imaging*, vol. 13, pp. 587–593, Apr. 1994.
[20] C. E. Hayes and P. B. Roemer, "Noise correlations in data simultaneously acquired from multiple surface coil arrays," *Magn. Res. Med.*, vol. 16, pp. 181–191, 1990.
[21] P. B. Roemer, W. A. Edelstein, C. E. Hayes, S. P. Souza, and O. M. Mueller, "The NMR phased array," *Magn. Res. Med.*, vol. 16, pp. 192–225, 1990.
[22] P. B. Roemer and W. A. Edelstein, "Ultimate sensitivity limits of surface coils," in *Proc. 6th Annu. Meet. Soc. Magn. Res. Med.*, New York, Aug. 1987, p. 410.
[23] J. Wang, A. Reykowski, and J. Dickas, "Calculation of the signal-to-noise ratio for simple surface coils and arrays of coils," *IEEE Trans. Biomed. Eng.*, vol. 42, pp. 908–917, Sept. 1995.
[24] A. Reykowski and S. M. Wright, "SNR for a idealized birdcage resonator and SNR limit for infinite cylindrical array," in *Proc. 3rd Annu. Meet. Soc. Magn. Res.*, Nice, France, Aug. 1995, p. 974.
[25] J. D. Jackson, *Classical Electrodynamics*, 2nd ed. New York: Wiley, 1975.
[26] C. T. Tai, *Dyadic Green Functions in Electromagnetic Theory*, 2nd ed. Piscataway, NJ: IEEE Press, 1994.
[27] R. E. Collin, *Field Theory of Guided Waves*. New York: IEEE Press, 1991.
[28] A. D. Poularkis and S. Seely, *Signals and Systems*. Boston, MA: PWD Engrg., 1985.
[29] D. Kress and R. Irmer, *Angewandte Systemtheorie*. München, Germany: Oldenburg, 1990.
[30] R. D. Stoy, K. R. Foster, and H. P. Schwan, "Dielectric properties of mammalian tissues from 0.1 to 100 MHz: A summary of recent data," *Phys. Med. Biol.*, vol. 27, no. 4, pp. 501–513, 1982.
[31] G. H. Glover, C. E. Hayes, N. J. Pelc, W. A. Edelstein, O. M. Mueller, H. R. Hart, C. J. Hardy, M. O'Donnell, and W. D. Barber, "Comparison of linear and circular polarization for magnetic resonance imaging," *J. Magn. Res.*, vol. 64, pp. 255–277, 1985.
[32] J. B. Kneeland, A. Jesmanovicz, and J. S. Hyde, "Depth sensitivity of single loop surface coils as a function of diameter and frequency," in *Proc. 7th Annu. Meet. Soc. Magn. Res. Med.*, San Francisco, CA, Aug. 1988, p. 866.
[33] L. C. Bourne, "Estimated SNR gains at 0.2 T from superconducting coils," in *Proc. 7th Annu. Meet. Int. Soc. Magn. Res. Med.*, San Francisco, CA, Aug. 1996, p. 1449.
[34] S. Serfaty, L. Darrasse, and S. Kan, "The pinpoint NMR coil," in *Proc. 2nd Annu. Meet. Soc. Magn. Res. Med.*, San Francisco, CA, Aug. 1994, p. 219.
[35] T. Antoniadis, S. Serfaty, and L. Darasse, "Optimum SNR with a dual surface coil," in *Proc. 4th Annu. Meet. Int. Soc. Magn. Res. Med.*, New York, Apr. 1996, p. 1429.
[36] W. Schnell, M. Vester, W. Renz, and H. Ermert, "The optimum geometry of the MR dual surface coil," in *Proc. 6th Annu. Meet. Int. Soc. Magn. Res. Med.*, Sydney, Australia, Apr. 1998, p. 2032.
[37] C. E. Hayes, W. A. Edelstein, J. F. Schenk, O. M. Mueller, and M. Eash, "An efficient, highly homogeneous radiofrequency coil for whole-body NMR imaging at 1.5 T," *J. Magn. Res.*, vol. 63, pp. 622–628, 1985.

Wilfried Schnell was born in Forchheim, Germany, in 1968. He received the Dipl. Ing. degree in electrical engineering from the University of Erlangen-Nuremberg, Germany, in 1993, and the Dr. Ing. degree from the Ruhr-University, Bochum, Germany, in 1997.

During internships at Siemens Medical Systems in Erlangen, Germany (1990–1992) and at the Danish Research Center of Magnetic Resonance at Hvidovre Hospital, Copenhagen, Denmark (1993), he optimized and developed RF equipment for magnetic resonance (MR) imaging and spectroscopy. From 1994 to 1996 he worked on general optimization of MR antennas using analytical and numerical methods at the Siemens Corporate Technology Group, Erlangen, Germany. In 1997, he joined the Siemens Information and Communication Networks Group, Munich, Germany, where he is responsible for electrical interconnection technologies. His interests include neural networks, electromagnetic field computations and their biomedical applications, electromagnetic interference and compatibility (EMI/EMC), electronics packaging and printed circuit board (pcb) technology, high-speed digital design, and signal integrity.

Dr. Schnell received the 1994 Electrical Engineering Diploma Award of the University of Erlangen-Nuremberg, Germany. He is a member of VDE/ITG (Germany).

Wolgang Renz was born in Regensburg, Germany, in 1957. He received the Dipl. Ing. (electrical engineering) and Dr. Ing. degrees from the University of Erlangen-Nuremberg, Germany, in 1983 and 1988, respectively.

From 1983 to 1988, he worked as a Research Assistant on RF and microwave discharges for gas laser excitation at the Laboratory for High-Frequency Technology, University of Erlangen-Nuremberg, Germany. After a Postdoctorate year at the Max Planck Institute for Plasma Physics, Garching, Germany, where he was working on RF and microwave discharges for surface treatment and material deposition, he joined Philips Kommunkations Industries, Nuremberg, Germany, in 1989, where he worked on fiber-optic communication equipment and application specific integrated circuits (ASIC's) for the synchronous digital hierarchy. In 1991 he joined the Siemens Corporate Technology Group, Erlangen, Germany, where he worked on RF antennas for MRI and general RF problems. In 1998 he moved to the MR Department, Siemens Medical Systems, where he is responsible for the development of transmit coils for MRI systems. His interests include the design and finite-element method calculation of RF structures and the power deposition in human tissue by RF fields.

Markus Vester was born in Sindelfingen, Germany, in 1958. He received the Dipl. Ing. degree in electrical engineering from the University of Erlangen-Nuremberg, Germany, in 1984, and the Dr. Ing. degree from the Ruhr-University, Bochum, Germany, in 1993.

In 1984, he joined Siemens Medical Systems, Erlangen, and since then he has been involved in the design of RF electronics and antennas for magnetic resonance imaging. From 1985 to 1992 he did experimental and theoretical research on microwave tomography at the Siemens Corporate Technology Group, Erlangen. His recent work there included the development of RF power amplifiers, a superconducting receive coil, and an ultrasound camera system. In his spare time, he enjoys homebrewing charge coupled device (ccd) cameras for amateur astronomy and longwave radio transmitters.

Helmut Ermert (M'79–SM'98) was born in Hagen, Germany, on April 2, 1941. He received the Dipl. Ing. (electrical engineering) degree and the Dr. Ing. degrees from the Technical University (RWTH), Aachen, Germany, in 1965 and 1970, respectively, and the Dr.-Ing. habil. degree (habilitation) from the Engineering Faculty at the University of Erlangen-Nuremberg, Germany, in 1975.

From 1966 to 1970, he worked on millimeter-wave and microwave engineering as a Research Assistant at the Institute of High-Frequency Engineering, Technical University (RWTH), Aachen. From 1970 to 1975 he was involved in teaching and research in microwave integrated circuits, microwave ferrites, and microwave measurement techniques as a Senior Scientist at the Institute of High Frequency Engineering, University Erlangen-Nuremberg. From 1978 to 1987 he was a Professor of electrical engineering in Erlangen, working on microwave and acoustic imaging. Since 1987 he has been a Professor of electrical engineering and Director of the High-Frequency Engineering Institute, Ruhr-University, Bochum, Germany. He is an associate editor of the journal *Biomedizinische Technik* (biomedical engineering). He is continuing research on measurement techniques, diagnostic imaging, and sensors in the RF and microwave area as well as in the ultrasonic area for applications in medicine, nondestructive testing, and industry.

Dr. Ermert is a member of VDE/ITG (Germany), German Society of Biomedical Engineering (DGBMT), German Society of Nondestructive Testing (DGZFP), German Society of Ultrasound in Medicine (DEGUM), Union Radio-Scientifique Internationale (URSI), and Commission B (elected member). From 1989 to 1991 he was an elected member of the Administrative Committee of the IEEE Ultrasonics, Ferroelectrics, and Frequency Control Society (Region 8) and since 1995 he has been an Associate Editor of the IEEE TRANSACTIONS ON ULTRASONICS, FERROELECTRICS AND FREQUENCY CONTROL. He was President of the DGBMT (1995–1997) and is currently President of the Umbrella Organization Medical Engineering (DVMT) in Germany.